High-Frequency EM Scattering by Edges in Artificially Hard and Soft Surfaces Illuminated at Oblique Incidence

Giuliano Manara, *Senior Member, IEEE*, Paolo Nepa, *Member, IEEE*, and Giuseppe Pelosi, *Fellow, IEEE*

***Abstract*—Uniform high-frequency expressions describing the field scattered by edges in anisotropic impedance surfaces illuminated at oblique incidence are provided. The specific anisotropic impedance boundary condition considered here exhibits a vanishing surface impedance along a principal anisotropy axis and an arbitrary one in the orthogonal direction. In certain circumstances, this tensor surface impedance may represent an accurate model for describing the scattering properties of artificially hard and soft surfaces. In order to simplify the analysis but without losing pertinence with real problems, in all canonical configurations we consider a face of the wedge to be perfectly conducting. The anisotropic impedance face is characterized by a tensor surface impedance with the principal anisotropy axes parallel and perpendicular to the edge.**

***Index Terms*—Anisotropic materials, artificial materials, electromagnetic edge diffraction, geometrical theory of diffraction.**

I. Introduction

ARTIFICIALLY hard and soft surfaces [1] are widely used in microwave technology as, for instance, in the design of hybrid-mode feed horns [2], radar calibrated targets [3], [4], and struts for minimum blockage width [5]. They are usually implemented either by suitably corrugating a metallic plane and then filling the corrugations with a dielectric material or by resorting to grounded dielectric slabs loaded by metallic strip gratings [6], [7].

The scattering properties of an infinite artificially hard or soft surface of the above kind can be analyzed by means of numerical techniques, taking advantage of the periodicity of the structure. However, from an engineering point of view, a problem of remarkable importance for the simulation of actual configurations is to account for the effects due to the finite extension of such surfaces. A rigorous solution for the scattering from finite artificially hard and soft surfaces can be obtained by applying the moment method (MM) to solve the integral equation for the currents on all material interfaces [6]. However, when the dimensions of the surface become much larger than the free-space wavelength, high-frequency techniques as for instance the uniform geometrical theory of diffraction (UTD) [8] represent a viable alternative to numerical approaches. Specifically, in the framework of a standard ray technique, the geometry of the actual scattering object can be locally approximated by resorting to canonical configurations and the scatterer material properties can be included in calculations by adopting approximate impedance boundary conditions (IBC's) [9].

In this context, suitable anisotropic IBC's have been proposed for modeling artificially hard and soft surfaces, when the period of the structure is much smaller than the free-space wavelength (the latter condition is usually met in practical applications). The corresponding surface impedance tensor exhibits a vanishing impedance value in the direction of corrugations or strips and a nonzero value (very high at those frequencies at which the artificial surface has been designed) in the orthogonal direction [9], [10]. Such a model has been applied for estimating the field reflected from radar polarimetric reflectors [11] and from a chiral slab backed by an artificially hard or soft surface [12]; also, it has been applied in conjunction with either an integral equation method or the UTD for evaluating the performance of elemental antennas on finite ground planes [6]. However, it is worth noting that the above anisotropic IBC model represents an accurate approximation only under specific conditions related to the direction of propagation of the incident plane wave [5]. IBC's depending on the direction of incidence [13] or of higher order [9] could provide a more realistic model, however rendering the attainment of the solution to the scattering problem much more cumbersome or even impossible. Nevertheless, we observe that the above uniform first-order IBC approximation exhibits a gradual loss of accuracy, eventually failing close to grazing incidence [6]. In the following, we adopt the above first-order anisotropic IBC model and apply it to analyze the scattering from truncations in artificially hard and soft surfaces.

The canonical problem relevant to the scattering of arbitrarily polarized plane waves obliquely incident on the edge of an anisotropic impedance wedge has not yet been analytically solved for the most general configurations. Several approximate analytical solutions and numerical techniques have been proposed in the literature (see [14] for a recent review on this subject). The difficulties encountered in analytical solution procedures are due to the fact that the IBC's holding on the wedge faces couple the longitudinal components of the electric and magnetic field, which are commonly used as potential functions to express all the other field components. The main

Manuscript received July 30, 1998; revised December 13, 1999.

G. Manara and P. Nepa are with the Department of Information Engineering, University of Pisa, I-56126 Pisa, Italy.

G. Pelosi is with the Department of Electronic Engineering, University of Florence, I-50134 Florence, Italy.

Publisher Item Identifier S 0018-926X(00)04369-6.

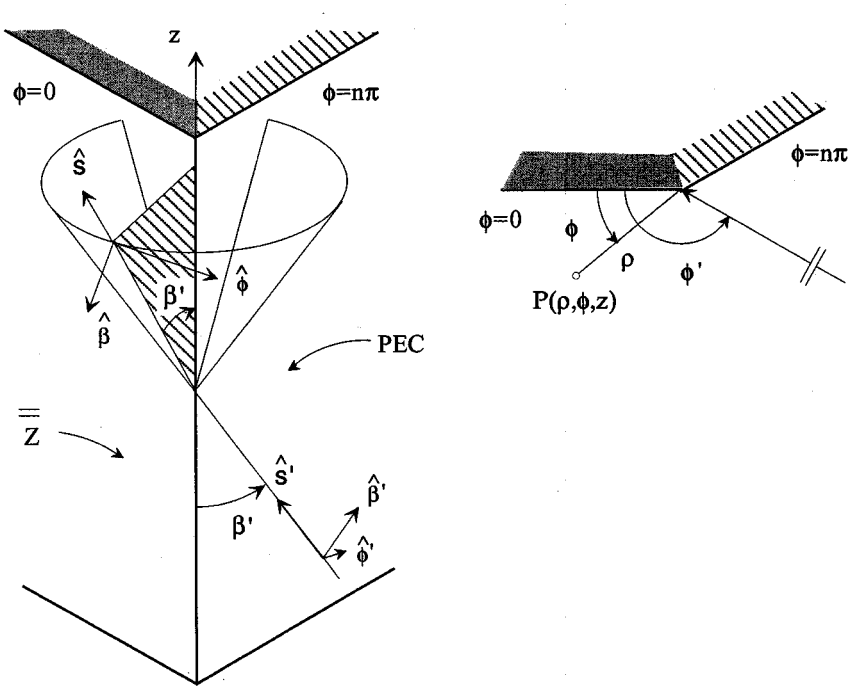

Fig. 1. Geometry for the scattering problem.

objective of this paper is to provide uniform high-frequency expressions for describing electromagnetic scattering from a class of anisotropic impedance wedges. In particular, the anisotropic faces are characterized by a tensor surface impedance with the principal anisotropy axes parallel and perpendicular to the edge of the wedge and exhibiting a vanishing surface impedance in one of the above principal directions. Such impedance tensors allow us to simulate edge effects in artificially hard and soft surfaces, when the direction of vanishing surface impedance is assumed to coincide with that of corrugations or strips, and a finite surface impedance value holds in the orthogonal direction.

Recently, rigorous integral solutions have been derived [15] for a set of specific wedge configurations, characterized by a perfect electric conducting (PEC) face and an anisotropic impedance face of the kind previously defined: 1) an arbitrary exterior angle wedge with a surface impedance tensor on the loaded face exhibiting a vanishing value in the direction parallel to the edge and 2) a half-plane, a full-plane, or a right-angled wedge with the anisotropic face exhibiting a vanishing surface impedance in the direction perpendicular to the edge. We observe that the solution procedure presented in [15] is only valid when the direction of vanishing surface impedance is either parallel or perpendicular to the edge. However, these specific configurations assume remarkable interest for applications. Moreover, work is in progress to extend the solution procedure to more general configurations, e.g., when the vanishing surface impedance direction is arbitrarily oriented with respect to the diffracting edge [16]. Uniform, high-frequency asymptotic expressions for the field components parallel to the edge are provided here for the above canonical anisotropic impedance wedge configurations, starting from the corresponding exact plane wave representations [15]; they include the standard Maliuzhinets special function [17]and the UTD transition function [8].

The paper has been organized as follows. The problem is formulated in Section II and uniform asymptotic expressions for the fields are given in Section III in the context of UTD. Then, samples of numerical results are presented in Section IV to demonstrate the effectiveness of the asymptotic expressions proposed, emphasizing at the same time the effects of anisotropy on the field scattered from the relevant impedance wedges. Finally, concluding remarks are drawn in Section V.

II. Statement of the Problem and Exact Spectral Representation for the Field

The geometry for the scattering problem is depicted in Fig. 1. The wedge has its edge on the z-axis of a standard cylindrical reference frame and the observation point is at $P \equiv (\rho, \phi, z)$. In all the configurations considered, the face $\phi = 0$ is characterized by a tensor surface impedance with the principal anisotropy directions parallel and perpendicular to the edge. Furthermore, we assume the face $\phi = n\pi$ to be perfectly conducting. The corresponding IBC's can be expressed as

$$E_\rho = Z_\rho H_z, \quad E_z = -Z_z H_\rho, \qquad \phi = 0 \tag{1a}$$

$$E_\rho = E_z = 0, \qquad \phi = n\pi \tag{1b}$$

with either $Z_z = 0$ or $Z_\rho = 0$. As noted in Section I, conditions (1a) are suitable to simulate the behavior of artificially hard and soft surfaces, when the direction of corrugations or strips is either parallel $(Z_z = 0)$ or perpendicular $(Z_\rho = 0)$ to the edge. Also, because of energy considerations $\mathrm{Re}\{Z_{\rho,z}\} \geq 0$.

An arbitrarily polarized plane wave impinges on the edge from a direction determined by the two angles β' and ϕ' (Fig. 1). The angle β' measures the incidence direction skewness with respect to the same edge ($\beta' = \pi/2$ in the normal incidence case). The unit vectors of the standard UTD *edge-fixed* coordinate system (Fig. 1) are defined by the following relationships: $\hat{e} = \hat{z}$, $\hat{\phi}' = (\hat{s}' \times \hat{e})/|\hat{s}' \times \hat{e}|$, $\hat{\phi} = -(\hat{s} \times \hat{e})/|\hat{s} \times \hat{e}|$, $\hat{\beta}' = \hat{\phi}' \times \hat{s}'$ and $\hat{\beta} = \hat{\phi} \times \hat{s}$. The longitudinal components of the incident field can be expressed as

$$\begin{aligned} E_z^i &= e_z \exp[-jkz\cos\beta'] \exp[ik_t\rho\cos(\phi - \phi')] \\ \zeta H_z^i &= h_z \exp[-jkz\cos\beta'] \exp[k_t\rho\cos(\phi - \phi')] \end{aligned} \quad (2)$$

where k and ζ are the wave number and intrinsic impedance of free-space, respectively, and $k_t = k\sin\beta'$ represents the transverse component of the wave vector. We note that $e_z = E_{\beta'}^i \sin\beta'$ and $h_z = -E_{\phi'}^i \sin\beta'$, where $E_{\beta'}^i$ and $E_{\phi'}^i$ are the electric field complex amplitude of a TM_z and a TE_z polarized incident plane wave, respectively, in the UTD *edge-fixed* coordinate system. An $\exp(j\omega t)$ time dependence has been assumed and suppressed.

Since the wedge structure is uniform along the z-axis, the scattered field exhibits the same $\exp(-jkz\cos\beta')$ dependence on z as the incident field in (2) that will be understood in the following. According to the Maliuzhinets method [17], [18], the total field in the presence of the wedge is written as

$$E_z = \frac{1}{2\pi j} \int_\gamma s_e(\alpha + \phi - n\pi/2) \exp[k_t\rho\cos\alpha]\, d\alpha \quad (3a)$$

$$\zeta H_z = \frac{1}{2\pi j} \int_\gamma s_h(\alpha + \phi - n\pi/2) \exp[k_t\rho\cos\alpha]\, d\alpha \quad (3b)$$

where $\gamma = \gamma^+ + \gamma^-$ is the two-fold Sommerfeld integration path shown in Fig. 2. In order to satisfy the radiation condition, the functions

$$s_e(\alpha) - \frac{e_z}{\alpha - (\phi' - n\pi/2)}$$

and

$$s_h(\alpha) - \frac{h_z}{\alpha - (\phi' - n\pi/2)}$$

must be regular in the strip $|\mathrm{Re}(\alpha)| \le n\pi/2$. Furthermore, the edge condition requires that $s_e(\alpha) = O(1)$ and $s_h(\alpha) = O(1)$, when $|\mathrm{Im}(\alpha)| \to \infty$.

Suitable expressions for the spectral functions will be given in this Section for all the configurations of interest previously described. The analytical procedure used to derive these spectral functions has been described in [15], where other anisotropic canonical problems have also been solved. We note that, since the spectral rigorous solutions provided here are defined along the Sommerfeld integration path, they are suitable for deriving incremental length diffraction coefficients (ILDC's) [19] or to develop accurate series representations for the description of the field in the vicinity of the edge.

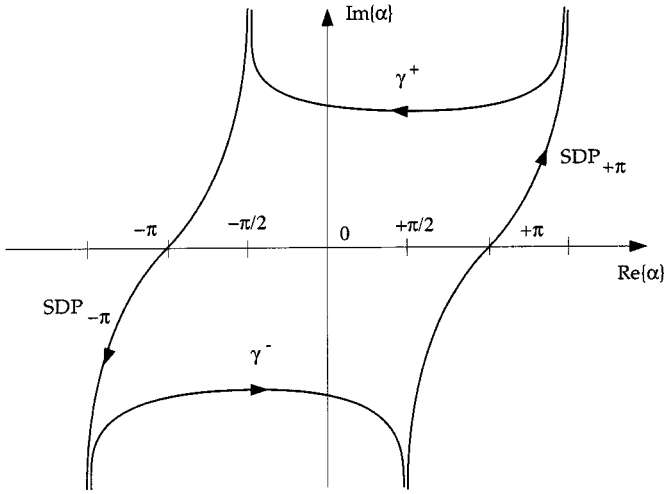

Fig. 2. Contours of integration on the complex plane.

A. $Z_z = 0$: *Arbitrary Exterior Angle Wedge*

In this case, the loaded face of the wedge ($\phi = 0$) is characterized by an impedance tensor exhibiting a vanishing surface impedance in the direction parallel to edge ($Z_z = 0$). An arbitrary value is assumed for Z_ρ. By defining

$$\psi(\alpha, \vartheta) = \psi_{n\pi/2}(\alpha + \vartheta - \pi/2)\psi_{n\pi/2}(\alpha - \vartheta + \pi/2) \quad (4)$$

where $\psi_{n\pi/2}(\alpha)$ is the Maliuzhinets special function [17], the spectral solution for the longitudinal field components can be expressed as

$$s_e(\alpha) = e_z \sigma_0(\alpha) \quad (5a)$$

$$s_h(\alpha) = \frac{\psi(\alpha - n\pi/2, \vartheta)\cos(\alpha/2n + \pi/4)}{\psi(\phi' - n\pi, \vartheta)\cos(\phi'/2n)}\, h_z \sigma_0(\alpha) \quad (5b)$$

where

$$\sigma_0(\alpha) = \frac{1}{n}\, \frac{\sin(\phi'/n)}{\sin(\alpha/n) + \cos(\phi'/n)} \quad (6)$$

and $\sin\vartheta = \sin\beta' Z_\rho/\zeta$. In the above expressions, ϑ is the Brewster angle for the TE_z polarization, with $0 \le \mathrm{Re}(\vartheta) \le \pi/2$ for lossy surfaces. We note that $\psi(\alpha, \vartheta)$ is free of poles and zeros in the strip $|\mathrm{Re}(\alpha)| \le n\pi$. Moreover, $\psi(\alpha, \vartheta) = O(\exp(|\mathrm{Im}(\alpha)|/2n))$ for $|\mathrm{Im}(\alpha)| \to \infty$, provided ϑ is finite, so that the edge condition is satisfied. As apparent from (5) the longitudinal components of the electric and magnetic fields are decoupled. We observe that $s_{e(\alpha)}$ in (5a) coincides with the electric field spectral function for a perfectly conducting wedge; this is also true for the magnetic field spectral function in (5b) when $Z_\rho = 0$. It is worth emphasizing that the spectral solutions in (5) are valid for arbitrary exterior wedge angles. We also note that an integral solution for the same problem but limited to the full plane configuration has been given in [20] by resorting to the Wiener–Hopf technique.

We finally observe that, in most cases, artificially hard and soft surfaces are modeled with a tensor surface impedance exhibiting a vanishing surface impedance in the direction of corru-

TABLE I
SOLVING SYSTEMS OF LINEAR EQUATIONS FOR DETERMINING THE CONSTANTS APPEARING IN THE RIGOROUS SPECTRAL SOLUTIONS FOR THE CONFIGURATIONS IN SECTION II-B

Configuration	constants	Solving system of linear equations
n=1	c_e, c'_e	$t_e(\pm\alpha_0 \mp \pi/2) = \mp j t_h(\pm\alpha_0 \mp \pi/2)$
n=2	c_e, c'_e, c''_e, c_h	$t_e(\pm\alpha_0 \mp \pi) = \mp j t_h(\pm\alpha_0 \mp \pi)$, $t_e(\pm\alpha_0) = \mp j t_h(\pm\alpha_0)$
n=1/2	c_e	$t_e(\alpha_0 - \pi/4) = -j t_h(\alpha_0 - \pi/4)$
n=3/2	c_e, c'_e, c_h	$t_e(\pm\alpha_0 - 3\pi/4) = \mp j t_h(\pm\alpha_0 - 3\pi/4)$ $t_e(\alpha_0 + \pi/4) = -j t_h(\alpha_0 + \pi/4)$

gations or strips and a very high surface impedance in the transverse direction [1], [6], [10]–[12]. The corresponding magnetic field spectral solution for the limit case ($Z_z = 0$, $Z_\rho \to \infty$) can be easily obtained from (5b) by taking into account that $\sin\vartheta \to \infty$ and $\psi(\alpha, \vartheta) \to 1$.

B. $Z_\rho = 0$: Full-Plane ($n = 1$); Half-Plane ($n = 2$); Interior ($n = 1/2$) and Exterior ($n = 3/2$) Right-Angled Wedges

In all the cases analyzed here the loaded face of the wedge ($\phi = 0$) is characterized by $Z_\rho = 0$. An arbitrary value is assumed for Z_z. The spectral solutions for the longitudinal field components can be expressed as

$$s_e(\alpha) = \Delta(\alpha)\{\cos\beta' \cos(\alpha + n\pi/2) t_e(\alpha) - \sin(\alpha + n\pi/2) t_h(\alpha)\} \tag{7a}$$

$$s_h(\alpha) = \Delta(\alpha)\{\cos\beta' \cos(\alpha + n\pi/2) t_h(\alpha) + \sin(\alpha + n\pi/2) t_e(\alpha)\} \tag{7b}$$

where

$$\Delta(\alpha) = \sin\beta'(1 - \sin^2\beta' \cos^2(\alpha + n\pi/2))^{-1}. \tag{8}$$

The corresponding expressions for $t_e(\alpha)$ and $t_h(\alpha)$ depend on the specific geometrical wedge configuration. In particular, for the full- and the half-plane ($n = 1, 2$)

$$t_e(\alpha) = e_x \sigma_0(\alpha) + c_e + c'_e \sin(\alpha/n) + c''_e \sin^2(\alpha/n) \tag{9a}$$

$$t_h(\alpha) = \frac{\Psi\left(\alpha - \frac{n\pi}{2}, \vartheta^+\right)\Psi\left(\alpha - \frac{n\pi}{2}, \vartheta^-\right)\cos(\alpha/2n + \pi/4)}{\Psi(\phi' - n\pi, \vartheta^+)\Psi(\phi' - n\pi, \vartheta^-)\cos(\phi'/2n)} \cdot (h_x \sigma_0(\alpha) + c_h) \tag{9b}$$

where $c2primes_e = c_h = 0$ if $n = 1$.

Conversely, for the right-angled configurations ($n = 1/2, 3/2$)

$$t_e(\alpha) = \frac{\cos(\alpha/2n + \pi/4)}{\cos(\phi'/2n)} \cdot (e_x \sigma_0(\alpha) + c_e + c'_e \sin(\alpha/n)) \tag{10a}$$

and

$$t_h(\alpha) = \frac{\Psi\left(\alpha - \frac{n\pi}{2}, \vartheta^+\right)\Psi\left(\alpha - \frac{n\pi}{2}, \vartheta^-\right)}{\Psi(\phi' - n\pi, \vartheta^+)\Psi(\phi' - n\pi, \vartheta^-)} \cdot (h_x \sigma_0(\alpha) + c_h) \tag{10b}$$

where $c'_e = c_h = 0$ if $n = 1/2$. In (9b) and (10b)

$$\sin\vartheta^\pm = \frac{\zeta/(Z_z \pm \sqrt{(\zeta/Z_z)^2 - 4\cos^2\beta'}}{2\sin\beta'} \tag{11}$$

with $0 \le \mathrm{Re}(\vartheta^\pm) \le \pi/2$. We note that $t_e(\alpha)$ and $t_h(\alpha)$ are the spectral functions for the integral representation of the transverse field components E_x and ζH_x, respectively, and the constants e_x, h_x represent the complex amplitudes of the x-components of the incident field [15]

$$e_x = (\sin\beta')^{-1}\{\cos\phi' \cos\beta' e_z + \sin\phi' h_z\} \tag{12a}$$

and

$$h_x = (\sin\beta')^{-1}\{\cos\phi' \cos\beta' h_z - \sin\phi' e_z\}. \tag{12b}$$

We also observe that for the configurations analyzed here, the IBC's expressed in terms of the x-components of the electric and magnetic field are decoupled on both wedge faces; moreover, $\vartheta^\pm$ denote the Brewster angles for a TE$_x$-polarized incident plane wave. The specific forms chosen for (9) and (10) guarantee the proper behavior of the spectral functions for $|\mathrm{Im}(\alpha)| \to \infty$. It is also important to note that the constants appearing in (9), (10) can be evaluated by solving a suitable system of linear equations (see Table I), where $\alpha_0 = j\ln(\tan(\beta'/2))$. This system is obtained by imposing the cancellation of the nonphysical poles introduced in (7) by the presence of $\Delta(\alpha)$ which is singular at $\alpha = \pm\alpha_0 - n\pi/2 + m\pi$, with $m = 0, \pm1, \pm2, \cdots$ [15].

In the limit case corresponding to the simplest model of an artificially hard or soft surface, i.e., $Z_\rho = 0$ and $Z_z \to \infty$, the Brewster angles defined in (11) become purely imaginary ($\vartheta^\pm = \mp\alpha_0$); the superscripts "+" and "−" denote the Brewster angles with a positive or negative imaginary part, respectively. In this case, the expressions for $t_e(\alpha)$ and $t_h(\alpha)$ strongly simplify since the term containing the Maliuzhinets special function

TABLE II
SOLVING SYSTEMS OF LINEAR EQUATIONS FOR DETERMINING THE CONSTANTS APPEARING IN THE RIGOROUS SPECTRAL SOLUTIONS FOR THE CONFIGURATIONS IN SECTION II-B IN THE LIMIT CASE $Z_s = 0$ AND $Z_z \to \infty$

Configuration	constants	Solving system of linear equations
n=1	c_e	$t_e(-\alpha_0 + \pi/2) = jt_h(-\alpha_0 + \pi/2)$
n=2	c_e, c'_e, c_h	$t_e(-\alpha_0 + \pi) = jt_h(-\alpha_0 + \pi)$, $t_e(\pm\alpha_0) = \mp jt_h(\pm\alpha_0)$
n=3/2	c_e, c_h	$t_e(\pm\alpha_0 + \pi/4) = \mp jt_h(\pm\alpha_0 + \pi/4)$

reduces to a trigonometric factor [15]. In particular, for the full- and the half-plane $(n = 1, 2)$ we obtain

$$t_e(\alpha) = \frac{\cos(\alpha_0/n) + \sin(\alpha/n)}{\cos(\alpha_0/n) - \cos(\phi'/n)} \cdot (e_x\sigma_0(\alpha) + c_e + c'_e \sin(\alpha/n)) \quad (13a)$$

$$t_h(\alpha) = \frac{(\cos(\alpha_0/n) + \sin(\alpha/n))\cos(\alpha/2n + \pi/4)}{(\cos(\alpha_0/n) - \cos(\phi'/n))\cos(\phi'/2n)} \cdot (h_x\sigma_0(\alpha) + c_h) \quad (13b)$$

where $c'_e = c_h = 0$ if $n = 1$. Conversely, when $n = 1/2, 3/2$

$$t_e(\alpha) = \frac{(\cos(\alpha_0/n) + \sin(\alpha/n))\cos(\alpha/2n + \pi/4)}{(\cos(\alpha_0/n) - \cos(\phi'/n))\cos(\phi'/2n)} \cdot (e_x\sigma_0(\alpha) + c_e) \quad (14a)$$

$$t_h(\alpha) = \frac{(\cos(\alpha_0/n) + \sin(\alpha/n))}{(\cos(\alpha_0/n) - \cos(\phi'/n))} \cdot (h_x\sigma_0(\alpha) + c_h) \quad (14b)$$

where $c_e = c_h = 0$ if $n = 1/2$. The constants appearing in (13) and (14) can be determined by resorting to the corresponding equations reported in Table II.

III. ASYMPTOTIC SOLUTION

By means of (3), the longitudinal field components E_z and ζH_z can be expressed in a form suitable for their uniform asymptotic evaluation with standard procedures [8] in the framework of UTD. In particular, by applying the residue theorem, the original integral representation for the total field along the Sommerfeld integration contour γ is reduced to the contribution of: two integrals defined along the steepest descent paths $SDP_{\pm x}$ through the saddle points at $\pm\pi$ (see Fig. 2); the residue of the poles which can be captured in the contour deformation process. Eventually we write

$$E_z = \sum_i \text{Re } s\{s_e(\alpha), \alpha = \alpha_i\} \cdot \exp[ik_t\rho\cos(\alpha_i - \phi + n\pi/2)] - \frac{1}{2\pi j}\int_{SDP_{\pm x}} s_e(\alpha + \phi - n\pi/2) \cdot \exp[jk_t\rho\cos\alpha]\, d\alpha \quad (15a)$$

and

$$\zeta H_z = \sum_i \text{Re } s\{s_h(\alpha), \alpha = \alpha_i\} \cdot \exp[jk_t\rho\cos(\alpha_i - \phi + n\pi/2)] - \frac{1}{2\pi j}\int_{SDP_{\pm\pi}} s_h(\alpha + \phi - n\pi/2) \cdot \exp[ik_t\rho\cos\alpha]\, d\alpha. \quad (15b)$$

Explicit closed-form expressions for any term appearing in (15) will be given in the following.

A. Geometrical Optics Field

The geometrical optics (GO) pole singularities are contained in the function $\sigma_0(\alpha)$, appearing in the expressions for $s_e(\alpha)$ and $s_h(\alpha)$ proposed for the different configurations. The residues of $s_e(\alpha)$ and $s_h(\alpha)$ at $\alpha_1 = \phi' - n\pi/2$ provide the contributions of the incident field in (2); they must be included in the solution if $\phi' - \pi < \phi < \phi' + \pi$. Moreover, the pole at $\alpha_2 = -\phi' - n\pi/2$ accounts for the field reflected from the anisotropic face $(\phi = 0)$. The expressions for the residue contributions associated with the latter pole include both a copolar and a cross-polar component

$$(E_z)_0^r = (R_{ee}(Z_\rho, Z_z)e_z + R_{eh}(Z_\rho, Z_z)h_z) \cdot \exp[ik_t\rho\cos(\phi + \phi')]U(\pi - \phi' - \phi) \quad (16a)$$

$$(\zeta H_z)_0^r = (R_{hh}(Z_\rho, Z_z)h_z + R_{he}(Z_\rho, Z_z)e_z) \cdot \exp[ik_t\rho\cos(\phi + \phi')]U(\pi - \phi' - \phi) \quad (16b)$$

where $U(\cdot)$ is the Heaviside unit step function. In particular, when the $\phi = 0$ face is characterized by $Z_z = 0$

$$R_{ee}(Z_\rho, Z_z = 0) = -1 \quad (17a)$$

$$R_{eh}(Z_\rho, Z_z = 0) = R_{he}(Z_\rho, Z_z = 0) = 0 \quad (17b)$$

$$R_{hh}(Z_\rho, Z_z = 0) = (\sin\phi' - \sin\beta' Z_\rho/\zeta))/(\sin\phi' + \sin\beta' Z_\rho/\zeta)). \quad (17c)$$

Conversely, when the $\phi = 0$ face is characterized by $Z_\rho = 0$

$$R_{ee}(Z_\rho = 0, Z_z) = \frac{(\sin\phi'(\sin\phi' - \sin\beta'/(Z_z/\zeta)) - \cos^2\beta'\cos^2\phi')}{(\sin\phi'\sin^2\beta'(\sin\phi' + 1/(\sin\beta' Z_z/\zeta)) + \cos^2\beta')} \tag{18a}$$

$$R_{eh}(Z_\rho = 0, Z_z) = -R_{he}(Z_\rho = 0, Z_z) = \frac{-\sin(2\phi')\cos\beta'}{(\sin\phi'\sin^2\beta'(\sin\phi' + 1/(\sin\beta' Z_z/\zeta)) + \cos^2\beta')} \tag{18b}$$

$$R_{hh}(Z_\rho = 0, Z_z) = \frac{(\sin\phi'(\sin\phi' + \sin\beta'/(Z_z/\zeta)) - \cos^2\beta'\cos^2\phi')}{(\sin\phi'\sin^2\beta'(\sin\phi' + 1/(\sin\beta' Z_z/\zeta)) + \cos^2\beta')}. \tag{18c}$$

It is worth noting that the previous expressions exactly recover those obtained by considering plane wave reflection from an infinite planar anisotropic impedance surface, as expected.

The pole at $\alpha_3 = -\phi' + 3n\pi/2$ accounts for the field reflected from the perfectly conducting face $\phi = n\pi$. The expressions for the corresponding residue contributions are

$$(E_z)_n^\pi = -e_z \exp[ik_t\rho\cos(\phi + \phi' - 2n\pi)] \cdot U(\phi' + \phi - (2n-1)\pi) \tag{19a}$$

$$(\zeta H_z)_n^\pi = h_z \exp[ik_t\rho\cos(\phi + \phi' - 2n\pi)] \cdot U(\phi' + \phi - (2n-1)\pi). \tag{19b}$$

Finally, we note that for geometrical configurations with $n < 1$ multiple reflections must also be accounted for [21]; moreover, the expressions in (17) and (18) can be easily extended to the limit cases $Z_\rho \to \infty$ and $Z_z \to \infty$, respectively.

B. Surface Waves

Surface waves can be supported only by the anisotropic impedance face. For those cases in which the nonvanishing surface impedance of the impedance tensor assumes a finite value, the poles associated with the surface wave contribution are introduced by the function defined in (4), which contains the Maliuzhinets special function. In particular, the spectral functions $s_e(\alpha)$ and $s_h(\alpha)$ exhibit a pole singularity at $\alpha_4 = -\pi - \vartheta_0 - n\pi/2$, with $\vartheta_0 = \vartheta$ when $Z_z = 0$ or $\vartheta_0 = \vartheta^\pm$ when $Z_\rho = 0$. The expressions for the residue contributions can be cast in the following form:

$$(E_z)_0^{sw} = C_e \exp[-jk_t\rho\cos(\phi + \vartheta_0)]U(\phi_{sw} - \phi) \tag{20a}$$

$$(\zeta H_z)_0^{sw} = C_h \exp[-jk_t\rho\cos(\phi + \vartheta_0)]U(\phi_{sw} - \phi) \tag{20b}$$

with $\phi_{sw} = gd(\mathrm{Im}(\vartheta_0)) - \mathrm{Re}(\vartheta_0)$, where $gd(x) = \mathrm{sgn}(x)\cos^{-1}(1/\cosh x)$ denotes the Gudermann function. It is apparent that the excitation condition requires $\phi_{sw} > 0$. When the face $\phi = 0$ is characterized by $Z_\rho = 0$, $\vartheta_0 = \vartheta^\pm$, but for lossy surfaces ($\mathrm{Re}\{Z_z\} \geq 0$), the two corresponding surface waves cannot satisfy the excitation condition simultaneously: just one of them can be supported by the loaded anisotropic face. The complex amplitudes of the surface wave contributions depend on the specific configuration analyzed. In particular, when $Z_z = 0$, with arbitrary values for Z_ρ and n, we obtain

$$\begin{aligned} C_e &= 0, \\ C_h &= \frac{C_0(\vartheta)\cos((\pi + \vartheta)/(2n))}{\psi(\phi' - n\pi, \vartheta)\cos(\phi'/(2n))} \cdot h_z\sigma_0(-\pi - \vartheta - n\pi/2) \end{aligned} \tag{21}$$

where

$$C_0(\vartheta_0) = -2n\sin\left(\frac{\pi}{2n}\right)\psi_{n\pi/2}(n\pi - \pi/2) \cdot \psi_{n\pi/2}(n\pi + \pi/2 + 2\vartheta_0). \tag{22}$$

In the limit case ($Z_z = 0$, $Z_\rho \to \infty$) surface waves do not exist on both wedge faces.

When the corrugations are perpendicular to the edge of the wedge, the surface wave amplitudes can be expressed as

$$C_e^\pm = -\Delta(-\pi - \vartheta^\pm - n\pi/2)\sin\vartheta^\pm C_x^\pm \tag{23a}$$

$$C_h^\pm = -\Delta(-\pi - \vartheta^\pm - n\pi/2)\cos\beta'\cos\vartheta^\pm C_x^\pm \tag{23b}$$

where $C_x^\pm$ are given in (24), shown at the bottom of the page, for the full-plane ($c_h = 0$ if $n = 1$) and the half-plane, and

$$C_x^\pm = \frac{C_0(\vartheta^\pm)\,(h_x\sigma_0(-\pi - n\pi/2 - \vartheta^\pm) + c_h)}{\Psi(\phi' - n\pi, \vartheta^+)\Psi(\phi' - n\pi, \vartheta^-)} \tag{25}$$

for the acute right-angled wedge configuration ($n = 3/2$).

It is worth noting that for any electrical configuration analyzed here, $C_e = C_h = 0$ if $n = 1/2$, as expected [21]; indeed, the Maliuzhinets special function does not contain pole singularities in the latter specific case.

$$C_x^\pm = \frac{C_0(\vartheta^\pm)\cos((\pi + \vartheta^\pm)/(2n))\,(h_x\sigma_0(-\pi - n\pi/2 - \vartheta^\pm) + c_h)}{\Psi(\phi' - n\pi, \vartheta^\pm)\Psi(\phi' - n\pi, \vartheta^-)\cos(\phi'/2n)} \tag{24}$$

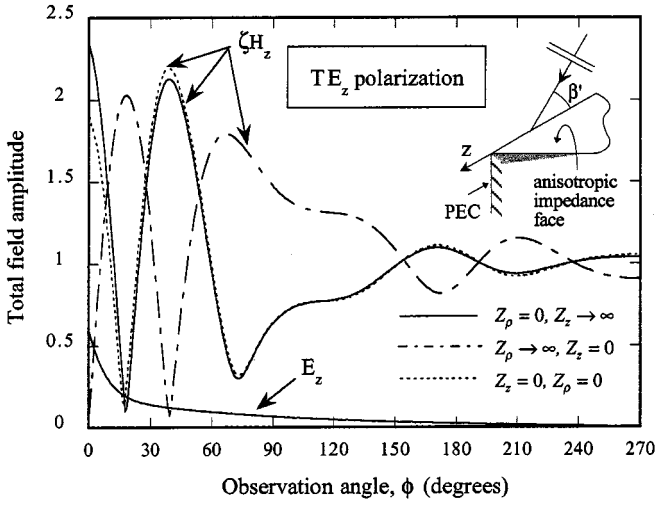

(a)

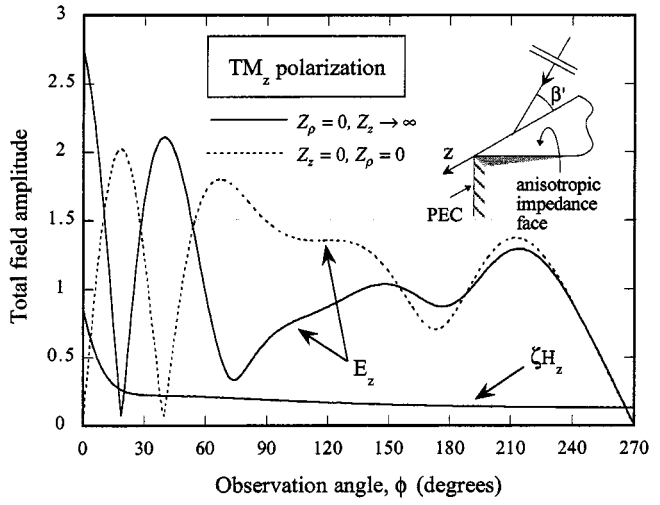

(b)

Fig. 3. Amplitude of the total field in the presence of a right-angled wedge illuminated by a plane wave at oblique incidence ($\phi' = \pi/2,\ \beta' = \pi/4$). The face $\phi = 3\pi/2$ is perfectly conducting. The field is evaluated at a constant distance from the edge ($k\rho \sin\beta' = 5$). (a) TE$_z$ polarization case. (b) TM$_z$ polarization case.

When $Z_\rho = 0$ and $Z_z \to \infty$ the Brewster angles defined in (11) are purely imaginary $\vartheta^{\pm} = \mp\alpha_0$; we note that $\alpha_4 = -\pi - \vartheta^{+} - n\pi/2 = -\pi + \alpha_0 - n\pi/2$ is the only pole which satisfies the excitation condition. This pole singularity is introduced in $s_e(\alpha)$ and $s_h(\alpha)$ by the term $\Delta(\alpha)$ defined in (8). Indeed, the constants contained in the spectral expressions (13) and (14) do cancel all the nonphysical poles introduced by $\Delta(\alpha)$, but α_4. The surface wave amplitudes assume the following form:

$$\begin{aligned} C_e &= t_h(-\alpha_0 - \pi - n\pi/2) \\ C_h &= jt_h(-\alpha_0 - \pi - n\pi/2) \end{aligned} \tag{26}$$

with $t_h(\alpha)$ given by (13b) and (14b), depending on the geometrical wedge configuration considered. Finally, we note that when $n = 1/2$ the surface wave contributions vanish, since $t_h(-\alpha_0 - 5\pi/4) = 0$.

C. Diffracted Field

The integrals along the $SDP_{\pm\pi}$ provide the contributions of the edge diffracted fields. Their accurate asymptotic evaluation [22] yields a uniform solution for the total field which is smooth and continuous at the shadow boundaries of the GO fields as well as at those of the surface waves. Indeed, all terms of order $K^{-1/2}$ (where $K = k_t\rho$ is the large parameter) must be retained [22] to obtain a uniform behavior of the field when the poles cross the integration path away from the saddle point; the latter situation verifies at the shadow boundaries of the surface waves propagating along the loaded face and excited at the edge by the diffraction phenomenon. The following uniform expressions for the longitudinal components of the diffracted fields are obtained

$$\begin{aligned} E_z^d = \frac{-e^{j\pi/4}e^{-jk_t\rho}}{\sqrt{2\pi k_t\rho}} \Bigg(& s_e(\pi + \phi - n\pi/2) \\ & - s_e(-\pi + \phi - n\pi/2) - \sum_i \operatorname{Re}\, s\{s_e(\alpha), \alpha = \alpha_i\} \\ & \cdot \frac{1 - F(\sqrt{k_t\rho[1 + \cos(\alpha_i - \phi + n\pi/2)]})}{2\cos[(\alpha_i - \phi + n\pi/2)/2]} \Bigg) \end{aligned} \tag{27a}$$

$$\begin{aligned} \zeta H_z^d = -\frac{e^{-j\pi/4}e^{-jk_t\rho}}{\sqrt{2\pi k_t\rho}} \Bigg(& s_h(\pi + \phi - n\pi/2) \\ & - s_h(-\pi + \phi - n\pi/2) - \sum_i \operatorname{Re}\, s\{s_h(\alpha), \alpha = \alpha_i\} \\ & \cdot \frac{1 - F(\sqrt{k_t\rho[1 + \cos(\alpha_i - \phi + n\pi/2)]})}{2\cos[(\alpha_i - \phi + n\pi/2)/2]} \Bigg) \end{aligned} \tag{27b}$$

where $F(\cdot)$ is the UTD transition function [8], generalized to complex argument as in [22], and the summation is extended to all poles included in the strip $|\mathrm{Re}(\alpha)| < 2\pi$ [22]. For practical applications, it is convenient to express the diffracted field in the *edge-fixed* coordinate system; since we assume to observe the field in the far-field region with respect to the diffraction point ($k_t\rho \gg 1$), the corresponding components can be easily derived from (27)

$$E_\beta^d = -E_z^d/\sin\beta', \quad E_\phi^d = \zeta H_z^d/\sin\beta'. \tag{28}$$

It is important to note that for the interior right-angled wedge ($n = 1/2$) the diffracted field contributions provided by the $SDP_{\pm\pi}$ integrals vanish, since the spectral representations for the longitudinal field components are periodic functions, with period 2π. As previously noted, the surface wave contributions vanish as well. Consequently, the total field rigorously coincides with that predicted by the GO solution, i.e., with the superposition of the incident field, the plane waves singly reflected from each face and a doubly reflected plane wave. In conclusion, in the interior right-angled wedge case ($n = 1/2$), the asymptotic evaluation of the rigorous spectral solution given here is in perfect agreement with the solution, which can be obtained by a direct application of the image principle [21].

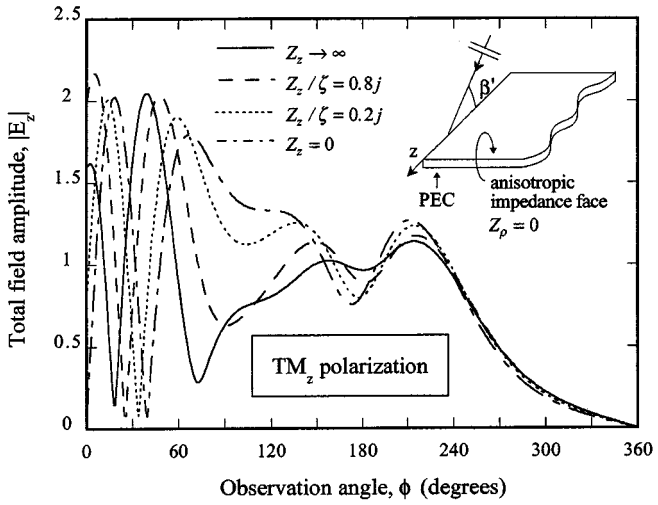

(a)

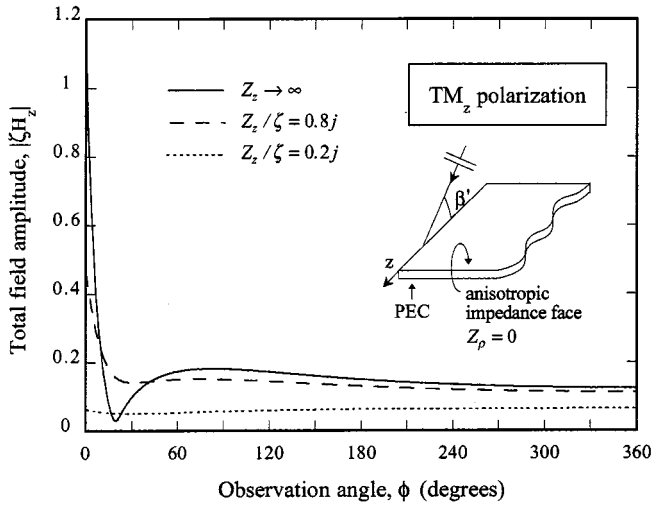

(b)

Fig. 4. Amplitude of the total field in the presence of an anisotropic impedance half-plane with a perfectly conducting face ($\phi = 2\pi$). The loaded face ($\phi = 0$) exhibits a vanishing surface impedance in the direction perpendicular to the edge ($Z_\rho = 0$). The half-plane is illuminated by a TM$_z$ polarized plane wave. Geometrical parameters: $k\rho \sin \beta' = 5$, $\beta' = \pi/6$, $\phi' = \pi/2$. (a) Copolar component (E_z). (b) Cross-polar component (ζH_z).

IV. Numerical Results

It is worth observing that extensive numerical tests were first performed to verify that the proposed solution recovers in the limit the solution for the corresponding perfectly conducting wedges, illuminated at oblique incidence [8]. Also, we numerically checked that at normal incidence our high-frequency expressions provide the same results as those obtained by a direct application of the exact Maliuzhinets solution valid for an isotropic impedance wedge [23]. Indeed, since the principal anisotropy directions are parallel and perpendicular to the edge, at normal incidence the general vector problem reduces to the superposition of two simpler scalar problems, whose solutions were given by Maliuzhinets in [17]. A sample of numerical results are shown in this section to demonstrate the effects on the scattered field introduced by the loaded face anisotropy.

The first example refers to a right-angled wedge illuminated by a plane wave impinging on the edge from $\phi' = \pi/2$, $\beta' = \pi/4$. The field is evaluated at a constant distance from the edge ($k\rho \sin \beta' = 5$). Both TE$_z$ ($e_z = 0, h_z = 1$) and TM$_z$ ($e_z = 1, h_z = 0$) polarization cases are considered in Fig. 3(a) and (b), respectively. The face $\phi = 3\pi/2$ is perfectly conducting. The continuous lines in Fig. 3(a) represent the amplitude of the copolar (ζH_z) and the cross-polar (E_z) components of the total field versus the observation angle ϕ, when the face $\phi = 0$ is loaded by an impedance tensor exhibiting a vanishing surface impedance in the direction perpendicular to the edge ($Z_\rho = 0$) and a diverging value along the direction of the edge ($Z_z \to \infty$). We note that these values of the anisotropic surface impedances can account for the presence of corrugations or strips perpendicular to the edge. Indeed, since the incident plane wave has its direction of propagation in the plane containing the edge and the normal to the anisotropic face, the impedance tensor provides an accurate model for an artificially soft surface [1]. As expected, the curve for the copolar component of the total field closely compares with that corresponding to the perfectly conducting right-angled wedge case (dotted line), except in the vicinity of the loaded face ($\phi = 0$) due to the presence of a surface wave. Also, the limit case ($Z_\rho \to \infty$, $Z_z = 0$) is considered in Fig. 3(a); for the specific incidence direction considered, the anisotropic face provides an accurate model for an artificially hard surface [1]. The dashed-dotted line describes the behavior of the amplitude of the total field copolar component (ζH_z); we note that the cross-polar component (E_z) exactly vanishes in the latter case, as well as in the case of the corresponding perfectly conducting wedge. Fig. 3(b) refers to the other polarization case (TM$_z$). In particular, the continuous lines describe the amplitude of the copolar and the cross-polar longitudinal components of the total field obtained by assuming $Z_\rho = 0$ and $Z_z \to \infty$ on the loaded face ($\phi = 0$). Again, the dotted line refers to the case of a perfectly conducting right-angled wedge. We note that the curve calculated for the copolar component of the total field (E_z) in the case ($Z_\rho \to \infty$, $Z_z = 0$) exactly overlaps with that for the perfectly conducting right-angled wedge; moreover, in both the latter cases the cross-polar components of the field rigorously vanish. We also point out that, when the face $\phi = 0$ of the wedge is characterized by ($Z_z \to \infty$, $Z_\rho = 0$), the plots for the co-polar components of the field in both Fig. 3(a) and (b) (ζH_z and E_z, respectively) exhibit a very similar behavior in a wide angular sector around the normal to the loaded face. This sector coincides with that region of space where the contributions from the incident and reflected field are dominant, in agreement with the reflecting properties of the artificial surface, which do not depend on polarization. A larger and larger disagreement is observed between the corresponding curves when the observation point moves toward the perfectly conducting face, where the contribution of the diffracted field becomes more and more important. Indeed, this field component must satisfy either Dirichlet or Neumann conditions at the face $\phi = 3\pi/2$, depending on the polarization. Similar considerations apply to the case in

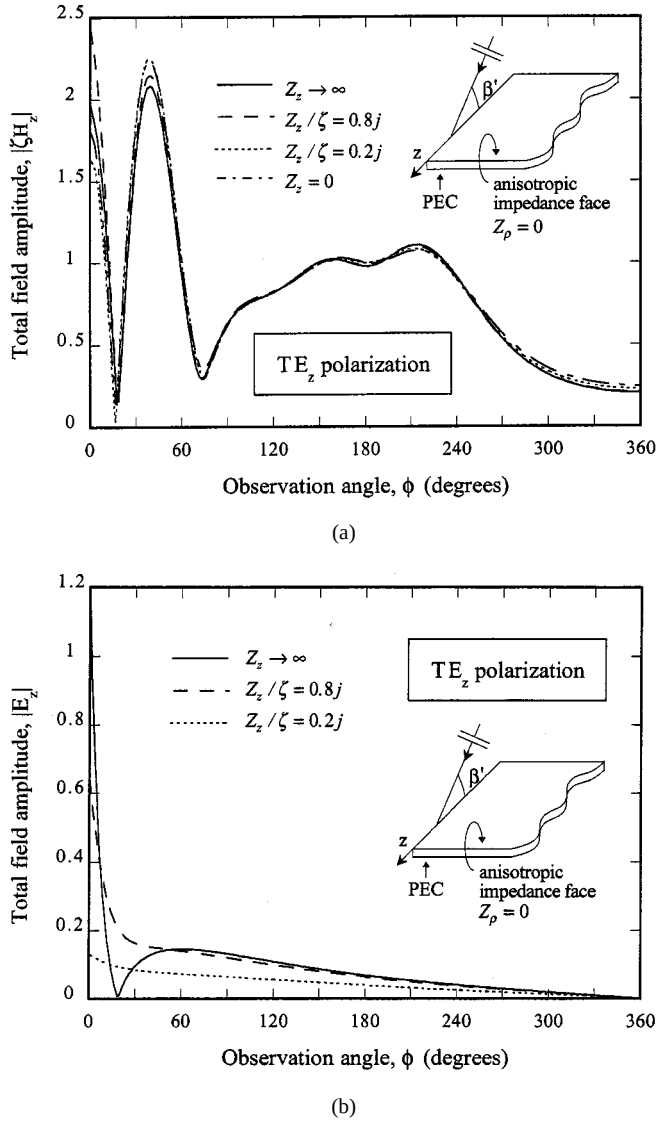

Fig. 5. Amplitude of the total field in the presence of an anisotropic impedance half-plane with a perfectly conducting face ($\phi = 2\pi$). The loaded face ($\phi = 0$) exhibits a vanishing surface impedance in the direction perpendicular to the edge ($Z_\rho = 0$). The half-plane is illuminated by a TE$_z$ polarized plane wave. Geometrical parameters: $k\rho \sin\beta' = 5$, $\beta' = \pi/6$, $\phi' = \pi/2$. (a) Copolar component (ζH_z). (b) Cross-polar component (E_z).

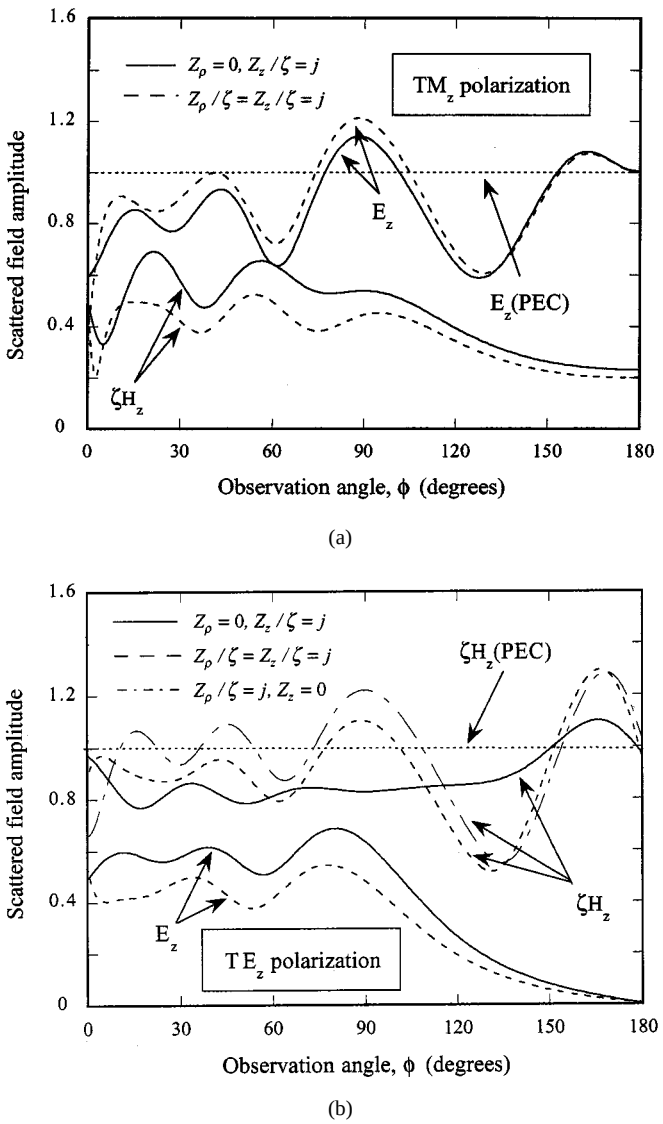

Fig. 6. Amplitude of the field scattered by an anisotropic impedance full plane with a perfectly conducting face ($\phi = \pi$). (a) TM$_z$ polarization case. (b) TE$_z$ polarization case. Geometrical parameters: $k\rho \sin\beta' = 10$; $\beta' = \pi/4$; $\phi' = \pi/3$.

which the loaded face is characterized by a tensor impedance with $Z_\rho \to \infty$, $Z_z = 0$ (compare dashed-dotted curve in Fig. 3(a) with dotted curve in Fig. 3(b).

A further example is shown in Fig. 4(a) and (b). The geometry of the scattering problem is sketched in the same figures; it consists of an anisotropic impedance half-plane with a perfectly conducting face ($\phi = 2\pi$). The field is calculated at a constant distance from the edge ($k\rho \sin\beta' = 5$). The half-plane is illuminated by a TM$_z$ polarized ($e_z = 1, h_z = 0$) plane wave impinging on the edge from $\beta' = \pi/6$, $\phi' = \pi/2$. The loaded face of the wedge ($\phi = 0$) exhibits a vanishing surface impedance in the direction perpendicular to the edge. Different plots are shown in both figures for different values of the normalized surface impedance in the direction of the edge (Z_z/ζ). The amplitude of the longitudinal copolar component (E_z) of the total field is shown in Fig. 4(a). In particular, the continuous line refers to the limit case ($Z_z \to \infty$); the dashed and the dotted lines correspond to different finite values of the longitudinal normalized surface impedance: $Z_z/\zeta = j0.8$ and $Z_z/\zeta = j0.2$, respectively. The dashed-dotted line has been plotted as a reference in the figure; it represents the case of a perfectly conducting half-plane. As apparent, starting from the curve for $Z_z \to \infty$, at the decreasing of the normalized surface impedance along the z-axis the curves for the field amplitude smoothly reduce to that for the perfectly conducting half-plane. The same consideration applies to Fig. 4(b), where curves for the amplitude of the cross-polar longitudinal field component (ζH_z) are plotted. We observe that the amplitude of the cross-polar field component becomes smaller and smaller at the decreasing of Z_z, eventually vanishing in the case of the perfectly conducting half-plane, as expected. The dual case of the TE$_z$ polarization ($e_z = 0, h_z = 1$) is reported in Fig. 5(a) and (b), where all the other

geometrical and electrical parameters coincide with those in Fig. 4(a) and (b). As far as the copolar component of the total field is concerned [Fig. 5(a)], we observe that for the polarization under test this component is not strongly affected by the value of the normalized surface impedance along the z-axis, except in the vicinity of the loaded face where the surface wave provides the dominant contribution to the field.

The last example refers to the case of a planar junction between an anisotropic impedance surface (face $\phi = 0$) and a perfectly conducting surface (face $\phi = \pi$). The full plane is illuminated by either a TM_z [Fig. 6(a)] or a TE_z [Fig. 6(b)] polarized plane wave, impinging on the edge from $\beta' = \pi/4$, $\phi' = \pi/3$. The scattered field is evaluated at a normalized distance $k\rho \sin\beta' = 10$. Several curves are plotted in both Fig. 6(a) and (b) with reference to different surface impedance tensors holding at the loaded face $(\phi = 0)$. In particular, the continuous lines in Fig. 6(a) refer to the copolar (E_z) and the cross-polar (ζH_z) components of the scattered field obtained in the case $(Z_\rho = 0, Z_z/\zeta = j)$; conversely, the dashed lines in the same figure represent the copolar (E_z) and the cross-polar (ζH_z) components of the scattered field in the case of an isotropic impedance face at $\phi = 0$: $Z_\rho/\zeta = Z_z/\zeta = j$. A further curve (dotted line) is plotted as a reference; it corresponds to the field reflected by a perfectly conducting plane. It is worth observing that in the latter case the cross-polar component (ζH_z) of the scattered field exactly vanishes. Similar considerations apply to the case reported in Fig. 6(b), where all electrical and geometrical parameters remain unchanged but the polarization, which is now TE_z. Again, the continuous and the dashed lines represent the behavior of the copolar (ζH_z) and the cross-polar (E_z) components of the scattered field when the surface impedances on the loaded face $(\phi = 0)$ assume the following values: $Z_\rho = 0$, $Z_z/\zeta = j$, and $Z_\rho/\zeta = Z_z/\zeta = j$, respectively. A further curve (dashed-dotted line) has been added to show the behavior of the copolar component (ζH_z) of the scattered field in the case: $Z_\rho/\zeta = j$, $Z_z = 0$ (the cross-polar component exactly vanishes). Again, the dotted line corresponds to the magnetic field amplitude of the plane wave reflected by a (PEC) plane.

V. Conclusion

A uniform high-frequency solution for the scattering by edges in anisotropic impedance surfaces illuminated at oblique incidence has been proposed, when the principal anisotropy axes are parallel and perpendicular to the edge. The specific anisotropic impedance boundary condition considered here exhibits a vanishing surface impedance along a principal anisotropy axis and an arbitrary one in the orthogonal direction. In certain circumstances, this surface impedance tensor may represent an efficient model for describing the scattering properties of artificially hard and soft surfaces. The uniform asymptotic expressions for the fields are given in a closed form containing the well-known Maliuzhinets special function. From a computational point of view, we observe that this solution exhibits the same numerical complexity as those previously derived for other specific impedance wedge configurations at oblique incidence.

References

[1] P.-S. Kildal, "Artificially soft and hard surfaces in electromagnetics," *IEEE Trans. Antennas Propagat.*, vol. 38, pp. 1537–1544, Oct. 1990.

[2] P. J. B. Clarricoats and A. D. Olver, *Corrugated Horns for Microwave Antennas*. London, U.K.: Peter Peregrinus Ltd., 1984.

[3] D. G. Michelson and E. V. Jull, "Depolarizing trihedral corner reflectors for radar navigation and remote sensing," *IEEE Trans. Antennas Propgat.*, vol. 43, pp. 513–518, May 1995.

[4] C. Gennarelli, G. Pelosi, and G. Riccio, "Physical optics analysis of the field backscattered by a depolarizing trihedral corner reflector," *Proc. Inst. Elect. Eng. Microwave, Antennas, Propagat.*, vol. 145, no. 3, pp. 218–231, June 1998.

[5] P.-S. Kildal, A. A. Kishk, and A. Tengs, "Reduction of forward scattering from cylindrical objects using hard surfaces," *IEEE Trans. Antennas Propagat.*, vol. 44, pp. 1509–1520, Nov. 1996.

[6] Z. Ying, P.-S. Kildal, and A. Kishk, "Study of different realizations and calculation models for soft surfaces by using a vertical monopole on a soft disk as a test bed," *IEEE Trans. Antennas Propagat.*, vol. 44, pp. 1474–1481, Nov. 1996.

[7] J. A. Aas, "Plane-wave reflection properties of two artificially hard surfaces," *IEEE Trans. Antennas Propagat.*, vol. 39, pp. 651–656, May 1991.

[8] R. G. Kouyoumijan and P. H. Pathak, "A uniform geometrical theory of diffraction for an edge in a perfectly conducting surface," *Proc. IEEE*, vol. 62, pp. 1448–1461, Nov. 1974.

[9] T. B. A. Senior and J. L. Volakis, *Approximate Boundary Conditions in Electromagnetics*. London, U.K.: Inst. Elect. Eng. Electromagn. Wave Ser. 41, 1995.

[10] Z. Sipus, H. Merkel, and P.-S. Kildal, "Grenn's functions for planar soft and hard surfaces derived by asymptotic boundary conditions," *Inst. Elect. Eng. Proc. Microwave, Antennas, Propagat.*, vol. 144, no. 5, pp. 321–328, 1997.

[11] I. V. Lindell and P. P. Puska, "Reflection dyadic for the soft and hard surface with application to the depolarising corner reflector," *Proc. Inst. Elect. Eng. Microwave, Antennas, Propagat.*, vol. 143, no. 5, pp. 417–421, Oct. 1996.

[12] A. J. Viitanen and P. P. Puska, "Reflection of obliquely incident plane wave from chiral slab backed by soft and hard surface," *Inst. Elect. Eng. Proc. Microwave, Antennas, Propagat.*, vol. 146, no. 4, pp. 271–276, Aug. 1999.

[13] G. Manara, P. Nepa, and G. M. Ottaviano, "A UTD solution for surface and leaky wave diffraction at the edge of a metallic wedge with a material coating," in *1996 IEEE AP-S Int. Symp. Dig.*, Baltimore, MD, July 1996, pp. 482–485.

[14] G. Pelosi, G. Manara, and P. Nepa, "Electromagnetic scattering by a wedge with anisotropic impedance faces," *IEEE Antennas Propagat. Mag.*, vol. 40, pp. 29–35, Dec. 1998.

[15] G. Manara, P. Nepa, and G. Pelosi, "EM scattering from anisotropic impedance wedges illuminated at oblique incidence. The case of artificially hard and soft boundary conditions," *Electromagn.*, vol. 18, no. 2, pp. 117–133, 1998.

[16] ——, "EM scattering by an anisotropic impedance half-plane with a perfectly conducting face illuminated at oblique incidence," in *USNC/URSI Radio Sci. Meet. Dig.*, Orlando, FL, July 1999, p. 91.

[17] G. D. Maliuzhinets, "Excitation, reflection and emission of surface waves from a wedge with given face impedances," *Sov. Phys. Dokl.*, no. 3, pp. 752–755, 1958.

[18] A. V. Osipov and A. N. Norris, "The Maliuzhinets theory for scattering from wedge boundaries: A review," *Wave Motion*, vol. 29, no. 4, pp. 313–340, 1999.

[19] G. Pelosi, S. Maci, R. Tiberio, and A. Michaeli, "Incremental length diffraction coefficients for an impedance wedge," *IEEE Trans. Antennas Propagat.*, vol. 40, pp. 1201–1210, 1992.

[20] A. H. Serbest, A. Buyukaksoy, and G. Uzgoren, "Diffraction by a discontinuity formed by two anisotropic impedance half planes," *Trans. IEICE*, vol. E-74, pp. 1283–1287, May 1991.

[21] T. Griesser and C. A. Balanis, "Reflections, diffractions, and surface waves for an interior impedance wedge of arbitrary angle," *IEEE Trans. Antennas Propagat.*, vol. 37, pp. 927–935, July 1989.

[22] R. G. Kouyoumjian, G. Manara, P. Nepa, and B. J. E. Taute, "The diffraction of an inhomogeneous plane wave by a wedge," *Radio Sci.*, vol. 31, no. 6, pp. 1387–1398, Nov./Dec. 1996.

[23] R. Tiberio, G. Pelosi, and G. Manara, "A uniform GTD formulation for the diffraction by a wedge with impedance faces," *IEEE Trans. Antennas Propagat.*, vol. 33, pp. 867–872, Aug. 1985.

Giuliano Manara (M'88–SM'93) was born in Florence, Italy, on October 30, 1954. He received the Laurea (Doctor) degree in electronics engineering (*summa cum laude*) from the University of Florence, Italy, in 1979.

Initially, he was with the Department of Electronics Engineering, University of Florence, as a Postdoctoral Research Fellow. In 1987 he joined the Department of Information Engineering, University of Pisa, where he works presently as a Full Professor. Since 1980 he has been collaborating with the Department of Electrical Engineering, The Ohio State University, Columbus, where, in the summer and fall of 1987, he was involved in research at the ElectroScience Laboratory. His current research interests include numerical and asymptotic techniques as applied to electromagnetic scattering and radiation problems (both in frequency and time domain), scattering from rough surfaces, and electromagnetic compatibility.

Paolo Nepa (M'95) was born in Teramo, Italy, in 1965. He received the Laurea (Doctor) degree in electronics engineering (*summa cum laude*), from the University of Pisa, Italy, in 1990.

Since 1990, he has been with the Department of Information Engineering, University of Pisa, where he is currently an Assistant Professor. In 1998 he was at the ElectroScience Laboratory (ESL), The Ohio State University, Columbus, as a Visiting Scholar supported by a grant of the Italian National Research Council. At the ESL he has been involved in research on efficient hybrid techniques for the analysis of large antenna arrays. His current research interests also include the extension of high-frequency asymptotic techniques to electromagnetic scattering from material structures.

Dr. Nepa received the Young Scientist Award from the International Union of Radio Science Commission B in 1998.

Giuseppe Pelosi (M'88–SM'91–F'00) was born in Pisa, Italy. He received the Laurea (Doctor) degree in physics (*summa cum laude*) from the University of Florence, Italy, in 1976.

Since 1979, he has been with the Department of Electronics and Telecommunications, University of Florence, where he is currently an Associate Professor of Microwave Engineering. He was a Visiting Scientist at McGill University, Montreal, Canada, in 1994 and 1995. He is coauthor of *Finite Elements for Wave Electromagnetics* (Piscataway, NJ: IEEE Press, 1994), *Finite Element Software for Microwave Engineering* (New York: Wiley, 1996), and *Quick Finite Elements for Electromagnetic Fields* (Norwood, MA: Artech House, 1998). His past research interests were focused on extensions and applications of the geometrical theory of diffraction as well as methods for radar cross section analysis of complex targets. He has been mainly involved in research in the field of numerical and asymptotic techniques for applied electromagnetics. His current research activity is mainly devoted to the development of numerical procedures in the context of the finite-element method, with particular emphasis on microwave and millimeter-wave engineering (antennas, circuits, devices, and scattering problems).

Dr. Pelosi is a member of the Board of Directors of the Applied Computational Electromagnetics Society.